Size distribution dependence of prion aggregates infectivity

Vincent Calvez [*†] Natacha Lenuzza [‡¶‖] Dietmar Oelz [§]
Jean-Philippe Deslys [†] Pascal Laurent [¶] Franck Mouthon [†‖]
Benoît Perthame [** ‖]

October 8, 2008

Abstract

We consider a model for the polymerization (fragmentation) process involved in infectious prion self-replication and study both its dynamics and non-zero steady state. We address several issues. Firstly, we extend a previous study of the nucleated polymerization model [16, 17] to take into account size dependent replicative properties of prion aggregates. This is achieved by a choice of coefficients in the model that are not constant. Secondly, we show stability results for this steady state for general coefficients where reduction to a system of differential equations is not possible. We use a duality method based on recent ideas developed for population models. These results confirm the potential influence of the amyloid precursor production rate in promoting amyloidogenic diseases. Finally, we investigate how the converting factor may depend upon the aggregate size. Besides the confirmation that size-independent parameters are unlikely to occur, the present study suggests that the PrPsc aggregate size repartition is amongst the most relevant experimental data to investigate this dependence. In terms of prion strain, our results indicate that the PrPsc aggregate repartition could be a constraint during the adaptation mechanism of the species barrier overcoming, that opens experimental perspectives for prion amyloid polymerization and prion strain investigation.

Key-words: Prion kinetics, polymerization process, size repartition, duality method.

1 Introduction

Transmissible spongiform encephalopathies (TSE) are fatal, infectious, neurodegenerative diseases. They include bovine spongiform encephalopathies (BSE) in cattle, scrapie in sheep and Creutzfeldt-Jakob disease (CJD) in human [1]. The infectious agents responsible for disease transmission, known as prions, present some unusual biological properties (as a high resistance to inactivation by heat or radiation). According to the "protein-only hypothesis", prions may consist in a misfolded protein (called PrPsc), without any nucleic acid. This

[*]Département de Mathématiques et Applications, École Normale Supérieure, CNRS UMR8553, 45 rue d'Ulm, F-75230 Paris cedex 05. Email: vcalvez@dma.ens.fr

[†]These authors contributed equally to this work

[‡]CEA-Institute of Emerging Diseases and Innovative Therapies, Route du Panorama, Bat. 60, F-92265 Fontenay-aux-Roses, Emails: natacha.lenuzza@cea.fr, franck.mouthon@cea.fr, jean-philippe.deslys@cea.fr

[§]Universität Wien, Fakultät für Mathematik, Nordbergstr. 15/C/7, 1090 Wien, Austria. Email: dietmar.oelz@univie.ac.at

[¶]Ecole Centrale Paris, Laboratoire MAS, Grande Voie des Vignes, F-92290 Châtenay-Malabry, Email: pascal.laurent@ecp.fr

[‖]These authors contributed equally to supervise this work

[**]Université Pierre et Marie Curie-Paris 6, UMR 7598 LJLL, BC187, 4, place Jussieu, F-75252 Paris cedex 5, and Institut Universitaire de France. Email: benoit.perthame@upmc.fr

hypothesis suggests that PrPsc replicates in a self-propagating process, by converting the normal form of PrP (called PrPc for Prion Protein cellular) into PrPsc (for Prion Protein scrappie) [2]. Many evidences are in favor of an autocatalytic replication of PrPsc, as the generation of infectivity from recombinant proteins [3] or the use of in vitro PrPsc conversion systems, such as the protein misfolding cyclic amplification (PMCA) technique [4].

However, the precise mechanism of conversion remains unclear. Moreover, prion infectious agent can exist under different strains, characterized by their incubation period and their lesion profile in brains [5]. In the framework of the protein-only hypothesis, it is supposed that strain diversity is supported by various conformation states of PrPsc, that leads to various biological and biochemical properties [6, 7]. A critical challenge of prion biology consists in elucidating the mechanism of conversion of PrPc into PrPsc, and therefore how a diversity of strains may exist in the same host (expressing the same PrP molecule).

To investigate the conversion of PrPc in PrPsc, many relevant mathematical modeling of prion replication have been proposed [8, 9, 10, 11]. Their major aim is to demonstrate that essential features of prion disease can be explained by purely physico-chemical mechanisms, as supposed by the protein-only hypothesis. In addition, mathematical modeling allows to study the effect of every elementary process in a separate manner [12], what is difficult to do experimentally.

The early proposed model is the heterodimer one. It is based on the conformational change of PrPc into PrPsc after the formation of a heterodimeric complex (PrPc + PrPsc $\rightarrow$ PrPc*PrPsc $\rightarrow$ PrPsc*PrPsc $\rightarrow$ 2 PrPsc). This model does not take into account the aggregation of PrPsc, and thereby fails to explain the association between infectivity and aggregated PrP. Some other mechanisms have been proposed, which are interested in PrP aggregation [9, 10, 13, 14, 15]. Based on fibrilar aggregation, the model which seems by now broadly accepted is the one of nucleated polymerization [9, 16, 17]. In this approach, PrPsc is considered to be a polymeric form of PrPc. Polymers can lengthen by addition of PrPc monomers, and they can replicate by splitting into smaller fragments. Greer et al. [18] recently improved the model to include a mean saturation effect by the whole population of polymers onto the lengthening process (called general incidence), and polymer joining (through a Smoluchowski coagulation equation). Another improvement is proposed in [19] where an intermediate state of converted PrP is introduced.

In these models, each aggregate has the same replicative behavior regardless to its size (modelled by constant kinetic parameters). However, some indirect evidences suggest that this hypothesis could be relaxed. Indeed, PrPsc aggregates are very heterogeneous in morphology: in several preparation conditions, either amorphous, spherical or fibrillar aggregates have been observed [20, 21, 22]. Moreover, the difficulties to generate infectivity from PrPsc with pure recombinant PrPc suggest that co-factors are necessary to the conversion mechanism of PrPc in infectious PrPsc (for instance, glycosaminoglycans may be important in the formation or stabilization of PrPsc [23]). A replication rate identical for every aggregate size, as supposed in previous models, would imply that interactions between PrPsc and other co-factors are structured-independent. However, it seems unlikely that differently structured aggregates possess the same biological or biophysical properties. More direct evidences are also in favor of a non constant behavior. Recent experimental analysis of relation between infectivity and size distribution of PrPsc aggregates (for PrPsc purified from infected brain [20] or for PrPsc produced by PMCA [24, 25]) contradicts this uniform behavior of PrPsc aggregates. For instance, Weber et al. found a bell-shaped-like dependence of infectivity on particle size in an infectivity assay using N2a cells [25, 26]. Taken together, these considerations suggest that the infectivity of PrPsc aggregates could be dependent on its aggregation state, i.e. its size in the theoretical systems.

The aim of our study is to generalize previous models to take into account the infectivity prion size-dependence. In mathematical models, infectivity is a balance between three ele-

mentary processes (namely fragmentation, degradation/sequestration and polymerization). Although we cannot exclude a size-dependent stability (assumed as a variable degradation rate or a variable fragmentation factor for large size), we have made the choice of a non-constant extension rate. Indeed, conversion activity, which is the most direct measure of our extension rate, is heterogeneous with regards to prion aggregates size [20, 27]. Furthermore, the hypothesis of a constant extension rate rests on the fibrillar aspect of PrPsc aggregates (i.e. polymerization occurs only at two ends of the polymer)[9, 16, 17]. However, so far, PrPsc-containing fibrils have not been found in infected brain tissues. The brain derived scrapie-associated fibrils (SAF) and Prion Rods may assemble during homogenization, extraction or purification and thus, be preparation artifacts [28, 29].

Thus, the major goal of the present work is to generalize Masel and coauthors' model of nucleated polymerization by taking a non-constant conversion rate, and to investigate the potential implications of the resulting prion aggregates size distribution in the strain phenomenon.

The paper is organized as follows: in section 2 we recall and review the model of Masel *et al.* and its continuous version [16] which is going to be used. We introduce our main improvement, namely a size-dependent lengthening factor related to nonuniform infectivity rate; and we discuss the eigenvalue problem which is a key tool to analyze the model. In section 3 we prove the stability of the zero steady state in the disease free regime (generalizing partially a result in [16]). Finally, in section 4 we study numerically the influence of different parameters on the dynamics of our model, in a prion strain perspective.

2 The continuum model

The following set of coupled differential equations has been introduced by Masel et al. [9] in order to model the polymerization (aggregation, fragmentation) process involved in infectious prion self-replication. It describes the dynamics of the quantity of PrPc $V(t)$, coupled with the evolution of aggregates of PrPsc $u_i(t)$ made of i elementary proteins,

$$\left\{\begin{array}{rcl} \dfrac{d}{dt}V(t) & = & \lambda - \gamma V(t) - \tau V(t)U(t) + 2\beta \displaystyle\sum_{i=1}^{n_0-1}\sum_{j>i} i u_j(t), \\ \dfrac{d}{dt}u_i(t) & = & -\mu u_i(t) - \beta(i-1)u_i - \tau V(t)(u_i(t) - u_{i-1}(t)) + 2\beta \displaystyle\sum_{j>i} u_j(t)\ , \quad \text{for } i \geq n_0\ . \end{array}\right. \tag{1}$$

The index n_0 denotes the minimal size of PrPsc polymers. The quantity $U(t) = \sum u_i(t)$ is the total amount of prion aggregates. The constant parameters $\lambda, \gamma, \tau, \beta, \mu$ are, respectively, the basal synthesis rate of PrPc, the degradation rate of PrPc, the conversion rate of PrPc into PrPsc (autocatalytic process following the mass action law), the fragmentation coefficient, and the degradation rate of PrPsc.

Analysis is simpler in the framework of continuous size of prions because analytical tools can serve to find simpler formulations. Accordingly, Greer *et al.* [16] introduce a continuous version of the discrete system (1) where they use the variable $x \in (0, +\infty)$ to denote the size of aggregates instead of the index $i \in \mathbb{N}$. This procedure can be justified by asymptotic derivations of continuous models from discrete models, see [30, 31]. The continuous model

reads, with possibly nonconstant coefficients,

$$\begin{cases} \dfrac{d}{dt}V(t) = \lambda - V(t)\left(\gamma + \displaystyle\int_{x_0}^{\infty} \tau(x)u(x,t)\,dx\right) + 2\int_0^{x_0} x \int_x^{\infty} \beta(y)\kappa(x,y)\,u(y,t)\,dy\,dx, \\ \dfrac{\partial}{\partial t}u(x,t) = -V(t)\dfrac{\partial}{\partial x}(\tau(x)u(x,t)) - [\mu(x)+\beta(x)]u(x,t) + 2\displaystyle\int_x^{\infty} \beta(y)\kappa(x,y)\,u(y,t)\,dy, \\ u(x_0,t) = 0, \end{cases} \tag{2}$$

together with appropriate initial conditions (*e.g.* $V_0 = \lambda/\gamma$, and $u_0(x)$ is a non-negative perturbation of the zero state) and with $u(x,t) = 0$ for $x \le x_0$. This is a well established family of models used for describing aggregation, fragmentation and possibly coagulation in polymer dynamics. It also appears in size structured cell dynamics with finite resources [32, 33, 34, 35]. Well-posedness, in the class of weak solutions, has been addressed by [36, 37, 38]. A general introduction to methods related to this type of model can be found in [39].

The transport term $V(t)\frac{\partial}{\partial x}(\tau(x)u(x,t))$ accounts for the growth in size of polymers by aggregation of converted normal proteins. Their size increases with the (extension) rate $V(t)\tau(x)$, proportional to the available PrPc molecules $V(t)$, with a conversion ability $\tau(x)$ depending on the size of the polymer according to the experimental evidences presented in the introduction. The fragmentation rate for a polymer of size y, is $\beta(y) > 0$. The repartition of the two fragments of (smaller) sizes x and $y - x$ is given by $\kappa(x,y) \ge 0$. It should thus satisfy the two usual laws [19, 33, 40] expressing that the number of fragments increases but keeping the total molecular mass unchanged (recall the factor 2 in the right hand side of (2))

$$\int_0^y \kappa(x,y)dx = 1\,, \qquad \int_0^y x\,\kappa(x,y)dx = \frac{y}{2}\,. \tag{3}$$

We may incorporate a minimal size of infectious PrPsc aggregates $x_0 \ge 0$, whose value remains unknown. Experimentally, no monomer of PrPsc has been isolated yet. In addition, small aggregates have been shown not to be infectious [20] (even-though they have to enter the actual modeling) and thus the assumption of a critical size of nucleation x_0 has been emphasized. However, the continuous model holds under the assumption that the monomer size can be neglected as opposed to possibly numerous large polymers (such that $x_0 \simeq 0$). Therefore we keep $x_0 \ge 0$ in the following but we sometimes neglect it ($x_0 = 0$) in order to simplify the presentation.

The system (2) keeps an important biochemical property: the prion molecules are properly transfered from one configuration to another (inducing no loss of mass during fragmentation or polymerization). This enhances the following macroscopic laws involving the total quantity of polymers $U(t)$ and the total mass of PrPsc fixed by the polymers $P(t)$ defined as

$$U(t) = \int_{x_0}^{\infty} u(x,t)dx \qquad P(t) = \int_{x_0}^{\infty} xu(x,t)dx. \tag{4}$$

In fact, using assumption (3), equation (2) yields the balance laws,

$$\frac{d}{dt}U(t) = \int_0^{\infty} [\beta(x) - \mu(x)]u(x,t)\,dx \qquad \text{(in the case } x_0 = 0),$$

$$\frac{d}{dt}\big(V(t) + P(t)\big) = \lambda - \gamma V(t) - \int_{x_0}^{\infty} x\mu(x)u(x,t)\,dx\,, \tag{5}$$

which asserts that the only possible creation or loss of PrP is due to the dynamics of PrPc (net production+degradation) and the natural sequestration of PrPsc.

General assumptions on the coefficients. In its entire generality, model (2) is rather difficult to attack even though some qualitative behaviors can be described as in section 3. We aim to reduce the complexity of this system in order to extract some relevant informations and concentrate on the conversion rate $\tau(x)$ for reasons mentioned earlier. At this stage of knowledge of the biochemical process, the available microscopic experimental data are insufficient to investigate different fragmentation laws in details. Indeed, we are not able to dissociate the three elementary processes (degradation/sequestration, splitting and polymerization) implicated in prion replication. We have made the choice of varying the conversion rate $\tau(x)$ as a first step, whereas Silveira *et al.* [20] clearly indicate that large polymers are more stable than small ones (this could be assumed as a reduced degradation rate or a saturated fragmentation factor for large sizes).

We recall a simple but natural choice for the coefficients, following [16]: the fragmentation rate is assumed to be proportional to the fragment size and the degradation rate does not depend of the size, that is,

$$\beta(x) = \beta_0 x\,, \qquad \mu(x) \equiv \mu_0\,, \tag{6}$$

and the probability distribution of fragments of size x is chosen to be uniform with respect to the length of the split polymers of size y:

$$\kappa(x,y) = \begin{cases} 0 & \text{if } y \le x_0 \ \text{ or } \ y \le x \\ 1/y & \text{if } y > x_0 \text{ and } 0 < x < y. \end{cases} \tag{7}$$

Last, but not least, the conversion rate $\tau(x)$ may also be assumed to be constant:

$$\tau(x) \equiv \tau_0. \tag{8}$$

In this situation the stable distribution of aggregates, as well as the possible asymptotic behaviors have been completely classified [9, 16] (see the last paragraph of this section). We refer to this choice (6)–(8) as the *constant coefficients case*.

With respect to previous modeling studies [9, 16], the main purpose of our work is to take into account more general assumptions for the coefficients. We explain how steady states can be obtained, and we partially analyze their stability properties. For the discussion, we focus on the case where only the conversion rate $\tau(x)$ differs from the "constant coefficients case". We try to foresee consequences in terms of qualitative behavior: which stable size distributions can be reached? What specific features do the dynamics exhibit? what are the possible biological interpretations?

A related eigenvalue problem. When $\mathbf{V}$ is frozen, it is convenient to introduce the aggregation/fragmentation operator

$$\mathcal{L}_{\mathbf{V}} u\,(x) := \mathbf{V}\frac{\partial}{\partial x}\big(\tau(x)u(x)\big) + \big(\mu(x)+\beta(x)\big)\,u(x) - 2\int_x^\infty \beta(y)\kappa(x,y)\,u(y)\,dy\,.$$

It has a dominant eigenvalue $\Lambda(\mathbf{V})$ (the opposite of the growth rate, also named *negative fitness* referring to population dynamics), associated to a nonnegative eigenfunction. In other words there is a unique solution $\mathcal{U}(\mathbf{V};x)$ to

$$\begin{cases} \mathcal{L}_{\mathbf{V}}\mathcal{U}(\mathbf{V};.)\,(x) = \Lambda(\mathbf{V})\,\mathcal{U}(\mathbf{V};x)\,, \\ \mathcal{U}(\mathbf{V};x_0) = 0\,, \quad \mathcal{U}(\mathbf{V};x) \ge 0\,, \quad \displaystyle\int_{x_0}^\infty \mathcal{U}(\mathbf{V};x)\,dx = 1\,. \end{cases} \tag{9}$$

Such solutions have been shown to exist, and the integrability condition implies an exponential decay at infinity, see [33, 34, 41].

These eigenelements help to give the qualitative behavior of the linear equation

$$\frac{\partial}{\partial t}u(x,t) + \mathcal{L}_{\mathbf{V}}u = 0\,.$$

It has been thoroughly studied using the Generalized Relative Entropy (GRE) method (see [33] and references therein). In a short, the distribution $u(x,t)$ tends to align along the dominant eigenfunction $\mathcal{U}(\mathbf{V};x)$ up to an exponential rescaling by the negative growth rate. It is proved that the time asymptotic regime is $u(x,t) \approx \varrho \exp(-\Lambda(V)t)\mathcal{U}(\mathbf{V};x)$ with ϱ a factor depending on the initial data. We refer to this regime as the "exponential phase".

We can derive a useful formula for the eigenvalue $\Lambda(\mathbf{V})$. The decay conditions at infinity ensure that the following integrations-by-parts can be justified (we assume $x_0 = 0$ below). Integrating (9) successively against 1 and x, gives

$$\begin{aligned}
&\int_0^\infty (\mu(x)+\beta(x))\,\mathcal{U}(\mathbf{V};x)\,dx - 2\int_0^\infty\int_x^\infty \beta(y)\kappa(x,y)\mathcal{U}(\mathbf{V};y)\,dy\,dx = \Lambda(\mathbf{V})\int_0^\infty \mathcal{U}(\mathbf{V};x)\,dx\,,\\
&-\mathbf{V}\int_0^\infty \tau(x)\mathcal{U}(\mathbf{V};x)\,dx + \int_0^\infty (x\mu(x)+x\beta(x))\mathcal{U}(\mathbf{V};x)\,dx\\
&\qquad\qquad - 2\int_0^\infty x\int_x^\infty \beta(y)\kappa(x,y)\mathcal{U}(\mathbf{V};y)\,dy\,dx = \Lambda(\mathbf{V})\int_0^\infty x\mathcal{U}(\mathbf{V};x)\,dx\ .
\end{aligned}$$

Using (3) we obtain as a direct consequence,

$$\Lambda(\mathbf{V}) = \int_0^\infty (\mu(x)-\beta(x))\,\mathcal{U}(\mathbf{V};x)\,dx = \frac{-\mathbf{V}\displaystyle\int_0^\infty \tau(x)\mathcal{U}(\mathbf{V};x)\,dx + \int_0^\infty x\mu(x)\mathcal{U}(\mathbf{V};x)\,dx}{\displaystyle\int_0^\infty x\mathcal{U}(\mathbf{V};x)\,dx}\,. \tag{10}$$

Discussion of the possible equilibria and corresponding dynamics. As pointed out already by [16], there are in general two steady states of the dynamics driven by (2). The first equilibrium is disease free, and we refer to it as the 'zero steady state':

$$\overline{V} = \frac{\lambda}{\gamma}\,, \quad \overline{u} \equiv 0\,. \tag{11}$$

As stressed in the setting of (2), we consider in general initial data which are close to this non-infected state. This results in an exponential phase after some transitory regime, the "pre-exponential phase". Indeed the linearized system around $(\overline{V},0)$ writes as follows (for $x_0 = 0$ and $\widetilde{V}(t) = V(t) - \overline{V}$),

$$\begin{cases}
\dfrac{d}{dt}\widetilde{V} = -\gamma\widetilde{V} - \overline{V}\displaystyle\int_0^\infty \tau(x)u(x,t)\,dx + \text{higher order terms}\,,\\
\dfrac{\partial}{\partial t}u(x,t) = -\mathcal{L}_{\overline{V}}u + \text{h.o.t.}\,.
\end{cases} \tag{12}$$

Due to the particular triangular form of the linearized problem, the principal eigenvalue $\Lambda(\overline{V})$ drives the growth of the system. It is thus a crucial quantity in order to get a qualitative picture of the system: is the disease free state stable or unstable (see Section 3)? What is the speed of the infection at early times (see Section 4 and Figure 3)? The early stages of infection are highly relevant biologically, because the observable quantities seem to be measured at the very beginning of the infection after inoculation. Discussing the biological implications of the current modeling (Section 4), we shall always assume we remain in the pre-exponential and exponential phases even though the full non-linear dynamics can be much more intricate.

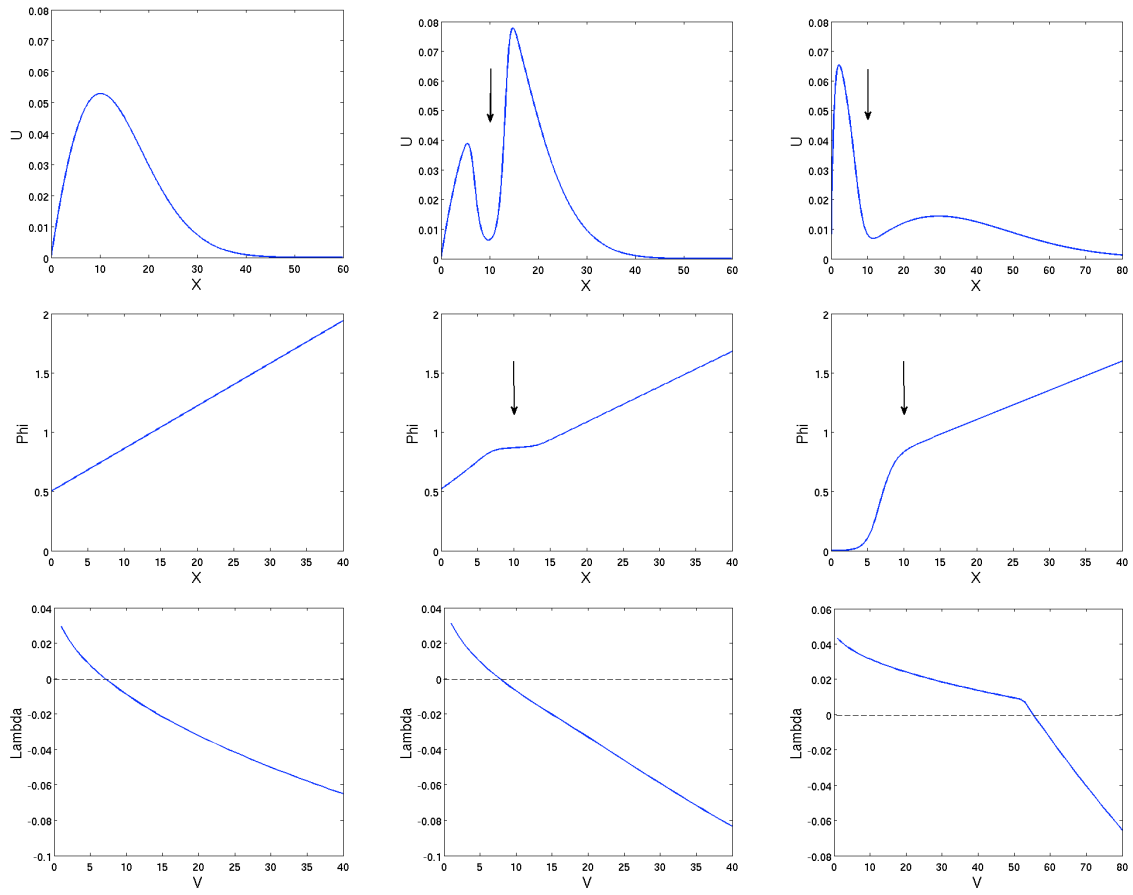

Figure 1: EIGENVALUE PROBLEM FOR THE MICROSCOPIC DISTRIBUTION. (top) Principal eigenfunction $\mathcal{U}(\mathbf{V};\cdot)$ solution of the problem (9) for respectively, a constant, a bell-shaped and a sigmoidal conversion factor $\tau(x)$. The arrow indicates the location of the sharp transition in the conversion factor $\tau(x)$. (middle) Corresponding adjoint eigenfunction $\varphi(\mathbf{V};\cdot)$ solution of the problem (19). Notice that it is in any case an increasing function, as assumed in Section 3. (bottom) Principal eigenvalue $\Lambda(\cdot)$ as a function of the PrPc (frozen) level $\mathbf{V}$. Observe that it is in any case a decreasing function, as assumed in Section 3. Coefficients are $\mu(x) \equiv 5.10^{-2}$, $\beta(x) = 3.10^{-2}x$, and respectively, $\tau(x) \equiv 1.10^{-2}$, $\tau(x) = 1.10^{-2} + 1.10^{-1}e^{-(x-10)^2/4}$ and $\tau(x) = 1.10^{-3} + 5.10^{-2}e^{x-10}/(1+e^{x-10})$. For the top and middle figures we set $\mathbf{V} = \overline{V} = 600$. Values are quoted from [12].

As we are also interested in long-time dynamics resulting in a balance between polymerization and fragmentation, we stress that another steady state (V_∞, u_∞) is possible for the system (2), being non trivial and satisfying:

$$\begin{cases} V_\infty \left(\gamma + \displaystyle\int_{x_0}^{\infty} \tau(x) u_\infty(x)\, dx \right) = \lambda + 2 \int_0^{x_0} x \int_x^\infty \beta(y)\kappa(x,y)\, u_\infty(y)\, dy\, dx\,, \\ V_\infty \dfrac{d}{dx}(\tau(x)u_\infty(x)) + (\mu(x)+\beta(x))\, u_\infty(x) = 2\displaystyle\int_x^\infty \beta(y)\kappa(x,y)\, u_\infty(y)\, dy\ , \end{cases} \tag{13}$$

with sufficient decay conditions at infinity. This nontrivial equilibrium ($u_\infty \not\equiv 0$) corresponds to the infection regime, and can be understood as follows. The equilibrium distribution u_∞ arises as an eigenfunction associated to the eigenvalue $\Lambda(V_\infty) = 0$ (9). In fact, this characterizes both the level of PrPc (V_∞) and the shape of the polymer distribution $\mathcal{U}(V_\infty; x)$. The complete description of the steady-state relies on knowing the total number of polymers. This missing factor is determined thanks to the first equation of (13). Interestingly enough, the value V_∞ does not depend on the differential equation driving $V(t)$. In particular it does not depend on λ and γ.

Consider the case $x_0 = 0$ for simplicity. The infectious steady state is given according to the rule:

$$\Lambda(V_\infty) = 0\,, \quad u_\infty(x) = \varrho_\infty \mathcal{U}(V_\infty; x)\ , \tag{14}$$

where ϱ_∞ denotes the total number of polymers. Such a steady state does not always exist [16]. In fact, according to the first equation of system (13), we have

$$V_\infty \left(\gamma + \varrho_\infty \int \tau(x) \mathcal{U}(V_\infty; x)\, dx \right) = \lambda\ ,$$

or, equivalently

$$\varrho_\infty = \frac{\lambda V_\infty^{-1} - \gamma}{\int \tau(x)\mathcal{U}(V_\infty; x)\, dx} > 0\ .$$

This points out a constraint for the non trivial steady state (V_∞, u_∞) to exist, namely it is required that

$$\gamma V_\infty < \lambda\,, \quad (\text{equivalently} \quad V_\infty < \overline{V})\,. \tag{15}$$

The stability of these steady states is one of the issues we address later.

The case of constant coefficients. For "constant coefficients" (6–8), the stability has been fully analyzed in [16, 17] and the situation is rather simple. As soon as the nontrivial equilibrium (V_∞, u_∞) exists, it is stable. Otherwise the disease free equilibrium is stable. This argument relies on the reduction of the infinite dimensional system to a three dimensional ordinary differential system on (U, P, V) due to remarkable cancellations.

We have the opportunity to recall their results under the viewpoint of the eigenvalue $\Lambda(\cdot)$ in (9). This eigenvalue can be explicitly computed from (10) which yields,

$$\Lambda(\mathbf{V}) = \mu_0 - \beta_0 \int_0^\infty x\mathcal{U}(\mathbf{V}; x)\, dx = \frac{-\tau_0 \mathbf{V} + \mu_0 \displaystyle\int_0^\infty x\mathcal{U}(\mathbf{V}; x)\, dx}{\displaystyle\int_0^\infty x\mathcal{U}(\mathbf{V}; x)\, dx}.$$

Eliminating the quantity $\int_0^\infty x\mathcal{U}(\mathbf{V}; x)dx = \sqrt{\tau_0 \mathbf{V}/\beta_0}$, we obtain

$$\Lambda(\mathbf{V}) = \mu_0 - \sqrt{\tau_0 \beta_0 \mathbf{V}}\ . \tag{16}$$

Notice that it is a decreasing function of $\mathbf{V}$ (this property is in fact crucial in the subsequent analysis).

We recover that the non-zero steady state corresponds to $V_\infty = \mu_0^2/(\tau_0\beta_0)$ and, following the constraint (15), it exists if and only if $\gamma\mu_0^2 < \lambda\tau_0\beta_0$. Then, the mean length of polymers is simply given:

$$\frac{\displaystyle\int_0^\infty x u_\infty(x)\,dx}{\displaystyle\int_0^\infty u_\infty(x)\,dx} = \frac{\mu_0}{\beta_0}. \tag{17}$$

From [16], we know that it is globally asymptotically stable. On the contrary, when it does not exist, the zero steady state is globally asymptotically stable.

3 Stability

We have seen previously that there are two possible steady states of the nonlinear system (2), setting the alternative between a disease free and an infected system and depending upon the prion production and degradation rates λ, γ. For "constant coefficients", Greer *et al.* [16] could study their stability using the possible reduction of the system to three coupled ordinary differential equations driving the macroscopic quantities $(V(t), U(t), P(t))$. Below we investigate the same question for more general coefficients. Our main assumption is the monotonicity property of the eigenvalue (9) which has been discussed above. This assumption is expected to be satisfied fairly generally (see Figure 1). We give in Subsection 3.3 below a class of coefficients for which we can indeed compute the eigenvalue and show that it is indeed decreasing. We set $x_0 = 0$ for the sake of simplicity throughout this section and assume

$$\text{The eigenvalue } \Lambda(\cdot) \text{ is a decreasing function of the (frozen) PrPc level } \mathbf{V}. \tag{18}$$

The adjoint problem. It emerges from the Generalized Relative Entropy method that the adjoint eigenvalue problem plays a central role when computing evolution of linearized problems, e.g., it defines the invariant measure of equation [33, 35]. As such it enters as a natural weight for various estimates. This problem reads as the following adjoint equation for the adjoint eigenfunction $\varphi(\mathbf{V}, x)$,

$$\begin{cases} -\mathbf{V}\tau(x)\dfrac{\partial}{\partial x}\varphi(\mathbf{V};x) + (\mu(x)+\beta(x))\,\varphi(\mathbf{V};x) - 2\displaystyle\int_0^x \beta(x)\kappa(y,x)\varphi(\mathbf{V};y)\,dy = \Lambda(\mathbf{V})\varphi(\mathbf{V};x)\ , \\ \varphi(\mathbf{V};x) \geq 0\,, \quad \displaystyle\int_0^\infty \mathcal{U}(\mathbf{V};x)\varphi(\mathbf{V};x)\,dx = 1\,. \end{cases} \tag{19}$$

The existence theory for such a problem has been addressed in [35] and we do not consider the question of existence problem. We state a series of useful (and reasonable) assumptions concerning this adjoint problem for computing purposes. Recall the notation $\overline{V} = \lambda/\gamma$ for the PrPc level at the disease free state (11). Recall also that the PrPc level at the conditional infected steady state, denoted as V_∞, is defined by $\Lambda(V_\infty) = 0$ according to (14). We denote $\overline{\varphi} = \varphi(\overline{V};\cdot)$ and assume that there are two constants K_1 and K_2 such that

$$\left|\tau(x)\frac{\partial}{\partial x}\overline{\varphi}(x)\right| \leq K_1\overline{\varphi}(x)\,, \quad \text{and} \quad \tau(x) \leq K_2\overline{\varphi}(x)\,. \tag{20}$$

This assumption generally holds true because $\overline{\varphi}$ grows linearly at infinity according to general abstract properties proved in [33, 35, 41]. See Figure 1 and Subsection 3.3 for explicit examples.

3.1 Stability of the zero state for $\overline{V} < V_\infty$

We first tackle the stability of the disease free steady state.

Theorem 1 (Local stability)**.** *Suppose that assumptions* (18) *and* (20) *hold true. Assume that* $\overline{V} < V_\infty$*. Then, in equation (2), the zero steady state* $(\overline{V}, 0)$ *is locally nonlinearly stable.*

We recall that in the case at hand ($\overline{V} < V_\infty$), there does not exist a non-zero steady state because (15) cannot be fulfilled with $\varrho_\infty > 0$.

Proof. According to Assumption (18), the condition $\overline{V} < V_\infty$ ensures that $\Lambda(\overline{V}) > 0$. We consider a perturbation of the ground state $V(t) = \overline{V} + \widetilde{V}(t)$ and $u(x,t) = 0 + \widetilde{u}(x,t)$ (note that $\widetilde{u}$ is nonnegative following the well-posedness theory in [36, 37], whereas we have no information concerning the sign of $\widetilde{V}$ *a priori*).

Because $\overline{V} = \lambda/\gamma$, the nonlinear system for this perturbation writes

$$\begin{cases} \dfrac{d}{dt}\widetilde{V}(t) = -\widetilde{V}(t)\left(\gamma + \displaystyle\int_0^\infty \tau(x)\widetilde{u}(x,t)\,dx\right) - \overline{V}\int_0^\infty \tau(x)\widetilde{u}(x,t)\,dx\,, \\ \dfrac{\partial}{\partial t}\widetilde{u}(x,t) = -\overline{V}\dfrac{\partial}{\partial x}(\tau(x)\widetilde{u}(x,t)) - \widetilde{V}(t)\dfrac{\partial}{\partial x}(\tau(x)\widetilde{u}(x,t)) - (\mu(x)+\beta(x))\widetilde{u}(x,t) \\ \qquad\qquad +2\displaystyle\int_x^\infty \beta(y)\kappa(x,y)\widetilde{u}(y,t)\,dy\,. \end{cases} \tag{21}$$

Following the duality method in [42], we test the equation on $\widetilde{u}$ in (21) against the adjoint eigenfunction $\overline{\varphi}$:

$$\frac{d}{dt}\int_0^\infty \widetilde{u}(x,t)\overline{\varphi}(x)\,dx = -\Lambda(\overline{V})\int_0^\infty \widetilde{u}(x,t)\overline{\varphi}(x)\,dx + \widetilde{V}(t)\int_0^\infty \left(\frac{\partial}{\partial x}\overline{\varphi}(x)\right)\tau(x)\widetilde{u}(x,t)\,dx\,.$$

On the other hand, multiplying the first differential equation in (21) by the sign of $\widetilde{V}$, we get:

$$\frac{d}{dt}|\widetilde{V}(t)| \le -|\widetilde{V}(t)|\left(\gamma + \int_0^\infty \tau(x)\widetilde{u}(x,t)\,dx\right) + \overline{V}\int_0^\infty \tau(x)\widetilde{u}(x,t)\,dx\,.$$

We obtain, choosing α large enough such that $\delta := \Lambda(\overline{V}) - K_2\overline{V}/\alpha > 0$,

$$\begin{aligned} &\frac{d}{dt}\left(\alpha\int_0^\infty \widetilde{u}(x,t)\overline{\varphi}(x)\,dx + |\widetilde{V}(t)|\right) \\ &\le -\alpha\Lambda(\overline{V})\int_0^\infty \widetilde{u}(x,t)\overline{\varphi}(x)\,dx + \alpha K_1|\widetilde{V}(t)|\int_0^\infty \widetilde{u}(x,t)\overline{\varphi}(x)\,dx \\ &\qquad\qquad -\gamma|\widetilde{V}(t)| - |\,\widetilde{V}(t)|\int_0^\infty \tau(x)\widetilde{u}(x) + K_2\overline{V}\int_0^\infty \widetilde{u}(x,t)\overline{\varphi}(x)\,dx \\ &\le -\min\left(\Lambda(\overline{V}) - \frac{K_2\overline{V}}{\alpha}, \gamma\right)\left(\alpha\int_0^\infty \widetilde{u}(x,t)\overline{\varphi}(x)\,dx + |\widetilde{V}(t)|\right) + \alpha K_1|\widetilde{V}(t)|\int_0^\infty \widetilde{u}(x,t)\overline{\varphi}(x)\,dx \\ &\le -\min(\delta,\gamma)\left(\alpha\int_0^\infty \widetilde{u}(x,t)\overline{\varphi}(x)\,dx + |\widetilde{V}(t)|\right) + \frac{K_1}{2}\left(\alpha\int_0^\infty \widetilde{u}(x,t)\overline{\varphi}(x)\,dx + |\widetilde{V}(t)|\right)^2. \end{aligned}$$

From this differential equation we conclude that, when $\alpha\int_0^\infty \widetilde{u}(x,t)\overline{\varphi}(x)dx + |\widetilde{V}(t)|$ is initially small enough, then the right hand side is negative. Therefore it decays for all times with the asymptotic exponential rate

$$\left(\alpha\int_0^\infty \widetilde{u}(x,t)\overline{\varphi}(x)\,dx + |\widetilde{V}(t)|\right) \le C_\varepsilon e^{-\big(\min(\delta,\gamma)-\varepsilon\big)t} \qquad \forall \varepsilon > 0\,.$$

□

We can also state the following variant of Theorem 1 under stronger assumptions.

Theorem 2 (Global stability)**.** *Additionally to the hypotheses of Theorem 1, assume that* $\tau(x) \geq k\overline{\varphi}(x)$ *for some constant* $k > 0$ *and that* $\overline{V}/\Lambda(\overline{V})$ *is small enough compared to* $k/(K_1K_2)$*. Then, in equation (2), the zero steady state* $(\overline{V}, 0)$ *is globally nonlinearly stable. In other words all solutions get extinct.*

As opposed to those of Theorem 1, the assumptions of Theorem 2 are difficult to check directly because the coefficients are intricate here. They mean that we are close to the case $\mu(x) \equiv \mu_0$, $\beta(x) \equiv \beta_1$ and $\tau(x) \equiv \tau_0$ because $\overline{\varphi}$ is constant in this case and therefore we can choose $K_1 = 0$ in Assumption (20) (see Subsection 3.3).

Proof. With these additional assumptions, we may keep one negative term in the last computation and arrive to,

$$
\begin{aligned}
&\frac{d}{dt}\left(\alpha\int_0^\infty \widetilde{u}(x,t)\overline{\varphi}(x)\,dx + |\widetilde{V}(t)|\right)\\
&\leq -\alpha\Lambda(\overline{V})\int_0^\infty \widetilde{u}(x,t)\overline{\varphi}(x)\,dx + \alpha K_1|\widetilde{V}(t)(t)|\int_0^\infty \widetilde{u}(x,t)\overline{\varphi}(x)\,dx\\
&\qquad\qquad - \gamma|\widetilde{V}(t)| - |\,\widetilde{V}(t)|\int_0^\infty \tau(x)\widetilde{u}(x,t) + K_2\overline{V}\int_0^\infty \widetilde{u}(x,t)\overline{\varphi}(x)\,dx\\
&\leq -\min\left(\Lambda(\overline{V}) - \frac{K_2\overline{V}}{\alpha}, \gamma\right)\left(\alpha\int_0^\infty \widetilde{u}(x,t)\overline{\varphi}(x)\,dx + |\widetilde{V}(t)|\right) + (\alpha K_1 - k)|\widetilde{V}(t)|\int_0^\infty \widetilde{u}(x,t)\overline{\varphi}(x)\,dx\\
&\leq -\min\left(\Lambda(\overline{V}) - \frac{K_2\overline{V}}{\alpha}, \gamma\right)\left(\alpha\int_0^\infty \widetilde{u}(x,t)\overline{\varphi}(x)\,dx + |\widetilde{V}(t)|\right).
\end{aligned}
$$

This last inequality will hold if we can find $\alpha > K_2\overline{V}/\Lambda(\overline{V})$ such that $\alpha K_1 < k$, which is precisely our smallness assumption. Then we have exponential decay of the solution. □

3.2 Persistence for $\overline{V} > V_\infty$

The same kind of method allows us to study the opposite case when another steady state exists. In this case we prove that the solution cannot go extinct using an argument initiated in [42]. We have the

Theorem 3 (Instability, persistence)**.** *Suppose again that assumptions* (18) *and* (20) *hold true. Assume that* $V_\infty < \overline{V}$*. Then the zero steady state* $(\overline{V}, 0)$ *is unstable in the sense that solutions cannot stay near* $(\overline{V}, 0)$ *for long times.*
Assume in addition that $K_1\overline{V} < \Lambda(\overline{V}) + \gamma$ *and that the initial perturbation satisfies* $V(0) \leq \overline{V}$*, then the solution persists: namely* V *stays away* $\overline{V}$ *and* $\int_0^\infty u(t,x)dx$ *stays away from* 0 *uniformly in time.*

Proof. We use the notations $v(t) = \overline{V} - V(t)$ and $w(t) = \int_0^\infty u(x,t)\overline{\varphi}(x)dx$ and the assumption $V_\infty < \overline{V}$ leads to $\Lambda(\overline{V}) < 0$.

To prove the first statement, we introduce ε_0 such that

$$
\frac{2K_1K_2\varepsilon_0\overline{V}}{\gamma + K_2\varepsilon_0} \leq |\Lambda(\overline{V})|\,. \tag{22}
$$

We shall prove that the subset

$$
\mathcal{S}_\varepsilon = \left\{(V,u)\,:\,|\overline{V} - V| < \frac{K_2\varepsilon\overline{V}}{\gamma + K_2\varepsilon} \text{ and } \int_0^\infty u(x)\overline{\varphi}(x)dx < \varepsilon\right\}
$$

is not stabilized accross the trajectories of (2) for any $\varepsilon <\varepsilon_0$. Following the proof of Theorem 1, we have on the one hand

$$\begin{aligned} &\frac{d}{dt}v(t) + \gamma v(t) = V(t)\int_0^\infty \tau(x)u(x,t)\,dx\,, \\ &0 \le \int_0^\infty \tau(x)u(x,t)\,dx \le K_2 w(t)\,. \end{aligned} \tag{23}$$

Consequently, for trajectories that remain in the set $\mathcal{S}_\varepsilon$ on the time interval $[t_0, t]$, we obtain the following estimate

$$0 \le \frac{d}{dt}v(t) + \gamma v(t) \le -K_2\varepsilon v(t) + K_2\varepsilon\overline{V}\,,$$

and thus

$$v(t_0)e^{-\gamma(t-t_0)} \le v(t) \le v(t_0)e^{-(\gamma+K_2\varepsilon)(t-t_0)} + \frac{K_2\varepsilon\overline{V}}{\gamma+K_2\varepsilon}\,, \qquad |v(t)| < \frac{2K_2\varepsilon\overline{V}}{\gamma+K_2\varepsilon}\,.$$

On the other hand, we can again combine the equation (19) defining the adjoint eigenfunction $\overline{\varphi}$ and the equation in (2) driving u, to obtain

$$\begin{aligned} \frac{d}{dt}w(t) &= -v(t)\int_0^\infty \tau(x)\frac{\partial}{\partial x}\overline{\varphi}(x)\,u(x,t)\,dx + |\Lambda(\overline{V})|w(t) \\ &\ge -K_1|v(t)|w(t) + |\Lambda(\overline{V})|w(t) \\ &\ge \left(-\frac{2K_1K_2\varepsilon\overline{V}}{\gamma+K_2\varepsilon} + |\Lambda(\overline{V})|\right)w(t) \\ &\ge 2K_1K_2\overline{V}\left(\frac{\varepsilon_0}{\gamma+K_2\varepsilon_0} - \frac{\varepsilon}{\gamma+K_2\varepsilon}\right)w(t)\,. \end{aligned} \tag{24}$$

Consequently, for $\varepsilon <\varepsilon_0$, the exponential growth induced by the differential inequality shows there is no way to ensure the condition $\int_0^\infty u(x,t)\overline{\varphi}(x)dx < \varepsilon$ for long time intervals. This proves the first statement.

In order to prove persistence of the solution, first examine (23): from the additional condition $V(0) \le \overline{V}$ we obtain that $v(t) > 0$ for all positive times. We can rewrite (23) and (24) as

$$\left\{\begin{array}{rcl} \dfrac{d}{dt}v(t) &\le& -\gamma v(t) + K_2\overline{V}w(t)\,, \\ \dfrac{d}{dt}w(t) &\ge& [-K_1v(t) + |\Lambda(\overline{V})|]w(t)\,. \end{array}\right.$$

Introduce the notation $\delta = \Lambda(\overline{V}) + \gamma - K_1\overline{V} > 0$. We compute the evolution of the ration between v and w:

$$\begin{aligned} \frac{d}{dt}\left(\frac{w(t)}{v(t)}\right) &\ge \frac{w(t)}{v(t)}\left(-K_1v(t) + |\Lambda(\overline{V})| + \gamma - K_2\overline{V}\frac{w(t)}{v(t)}\right) \\ &\ge \frac{w(t)}{v(t)}\left(\delta - K_2\overline{V}\frac{w(t)}{v(t)}\right)\,, \end{aligned}$$

from which we deduce the uniform bound from below: $w(t)/v(t) \ge \min(w(0)/v(0), \delta/(K_2\overline{V}))$. Notice that $w(t)$ lies asymptotically above $\delta/\overline{V}$. Consequently we have,

$$\begin{aligned} &\frac{d}{dt}w(t) \ge w(t)\left(|\Lambda(\overline{V})| - \frac{K_1}{\min(w(0)/v(0), \delta/(K_2\overline{V}))}w(t)\right)\,, \\ &w(t) \ge \min\left(w(0), \frac{|\Lambda(\overline{V})|\min(w(0)/v(0), \delta/(K_2\overline{V}))}{K_1}\right)\,. \end{aligned}$$

Therefore the initial perturbation persists away from the disease-free stationary state. □

3.3 A class of examples

In order to clarify the assumptions and properties stated before, we give a class of coefficients in equation (2) where the different eigenelements can be explicitly computed. In each case we will see that $\Lambda(\mathbf{V})$ is indeed a decreasing function of $\mathbf{V}$ (Assumption (18)), and that Assumption (20) reduces to the fact that $\tau(x)$ is bounded.

We first report from [33, 41] the case where $\tau(x) \equiv \tau_0$, $\mu(x) \equiv \mu_0$ and $\beta(x) \equiv \beta_1$ are constants. We obtain the solution to the adjoint problem (19),

$$\Lambda(\mathbf{V}) = \beta_1\,, \quad \varphi(\mathbf{V}; x) \equiv 1\,.$$

The eigenlements are usually difficult to evaluate in the direct problem (9) but can be easily computed in the adjoint equation (19). Indeed, searching for an affine solution $\varphi(\mathbf{V}; x) = 1 + x/L$, we find, using the structure properties of $\kappa(x, y)$ (3),

$$-\frac{\mathbf{V}\tau(x)}{L} + \mu(x)\left(1 + \frac{x}{L}\right) - \beta(x) = \Lambda(\mathbf{V})\left(1 + \frac{x}{L}\right)\,. \tag{25}$$

Hence another class where one can compute $\Lambda(V)$ corresponds to $\beta(x) = \beta_0\, x$, and $\tau(x) \equiv \tau_0$, $\mu(x) \equiv \mu_0$ are constant (the "constant coefficients case"). We get first

$$-\beta_0 L^2 + \tau_0\, \mathbf{V} = 0\,.$$

Therefore we obtain $L(\mathbf{V}) = \sqrt{\tau_0 \mathbf{V}/\beta_0}$ and $\Lambda(\mathbf{V}) = \mu_0 - \beta_0 L(\mathbf{V})$, as in Section 2. Observe that $\Lambda(\mathbf{V})$ is a decreasing function of $\mathbf{V}$ as asserted in Assumption (18).

We leave to the reader to check that $\Lambda(\mathbf{V})$ is also decreasing for the more general situation where $\beta(x) = \beta_1 + \beta_0 x$, $\tau(x) = \tau_0 + \tau_1 x$ and $\mu(x) \equiv \mu_0$ is constant. Indeed we deduce from (25) the following two relations:

$$\Lambda(\mathbf{V}) - \mu_0 + \frac{\mathbf{V}\tau_0}{L} + \beta_1 = 0\,, \quad \text{and} \quad \frac{\Lambda(\mathbf{V}) - \mu_0}{L} + \frac{\mathbf{V}\tau_1}{L} + \beta_0 = 0\,.$$

And thus $Z = \Lambda(\mathbf{V}) - \mu_0$ solves

$$(Z + \beta_1)(Z + \mathbf{V}\tau_1) = \mathbf{V}\tau_0\beta_0\,, \quad Z + \beta_1\,,\, Z + \mathbf{V}\tau_1 < 0\,,$$

the last constraint being due to the condition $L > 0$.

More generally, observe from (10) that the following conditions are fulfilled:

$$\Lambda(0) = \mu_0\,, \qquad \Lambda(\mathbf{V}) \leq \mu_0\,.$$

Notice that the problem for $\mathbf{V} = 0$ is degenerate and that the eigenfunction is singular at $x = 0$ [32].

On the other hand, we deduce for the same reason that, if $\min \tau(x)/x > 0$, then we have

$$\Lambda(\infty) = -\infty\,.$$

Consequently there exists at least one non-zero steady state.

4 Non-constant conversion rate and PrPsc aggregate size-distribution

The microscopic parameters of the model are quite difficult to assess experimentally, whereas the macroscopic outputs of our model (i.e. namely the kinetics of PrPsc accumulation or the PrPsc aggregate repartition according to their size) can be obtained more easily. We aim to gain some insight into reasonable scenarios for the converting activity through a macroscopic procedure. In particular we aim to understand how the conversion factor $\tau(x)$ may depend upon the aggregate size. This question is fully motivated by recent studies which clearly account for such an influence of the polymer length [20, 27]. Since the actual size distribution of the conversion factor $\tau(x)$ is still unknown, several size dependences have been tested and are depicted in Figure 2.

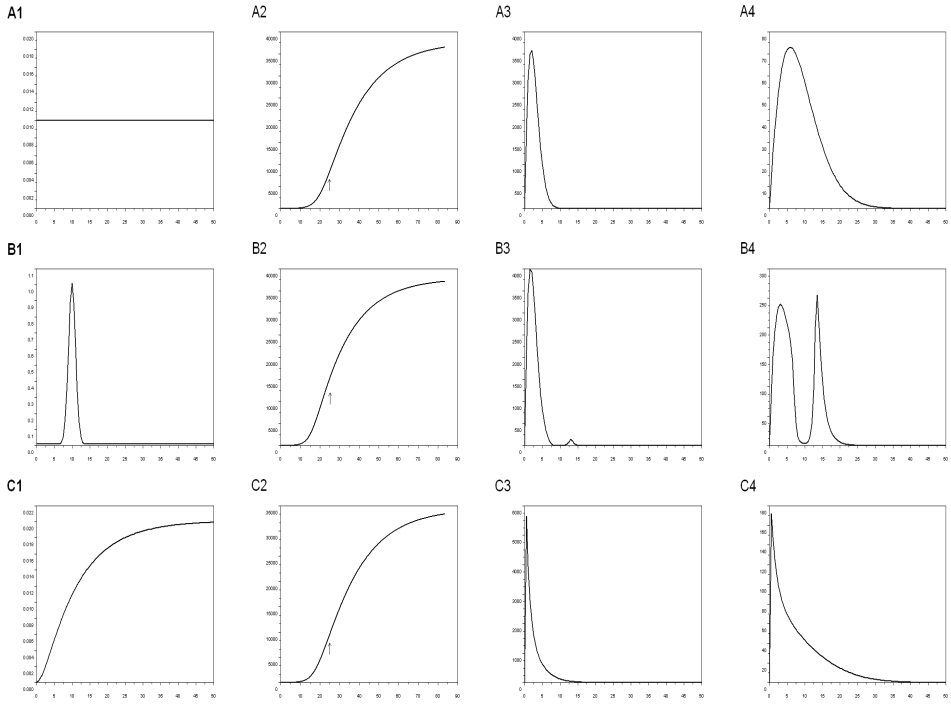

Figure 2: Prion replication for various size-dependent conversion rate $\tau(x)$. Three different shapes are depicted here : (A) a constant conversion rate $\tau = 0.01$, (B) a bell-shaped conversion rate $\tau = 0.01 + \exp(-0.5 * (x - 10)^2)$ and (C) a sigmoidal conversion rate $\tau = 0.0001 + 0.02 * (1 + 1/(10 - 2) * (2 * \exp(-x/2) - 10 * \exp(-x/10)))$, where x stands for aggregate size. The other parameters are kept constant and have been quoted from Rubenstein et al. [12] : $\lambda = 2400$ per day, $\gamma = 4$ per day, $\mu = .047$ per day, and $\beta = 0.03 * x$ per day. (A1, B1, C1) Size distribution of τ (abscissa = PrPsc aggregates size; ordinate = rate τ). (A2, B2, C2) Time evolution of total PrPsc amount (abscissa = Time (in days) ; ordinate = PrPsc (per day). The arrow represents time t=25 days, the end of the exponential phase of growth of PrPsc. (A3, B3, C3) PrPsc aggregates size distribution at equilibrium. (abscissa = PrPsc aggregates size; ordinate = PrPsc aggregates number). (A4, B4, C4) PrPsc aggregates size distribution at t=25 days.(abscissa = PrPsc aggregates size; ordinate = PrPsc aggregates number).

4.1 Total PrPsc accumulation

First, we can observe in Figure 2 that for a given initial PrPsc aggregate size, kinetic PrPsc accumulation profiles (i.e. $P(t)$) are similar, and thus, cannot be used to distinguish between a constant, a bell-shaped or a sigmoidal conversion factor $\tau(x)$ (all the other coefficients remaining equal).

We have also load the evolution problem (2) with a very peculiar initial condition being localized at a given length y_0, with a normalized quantity of PrPsc. The total amount of PrPsc obtained in a fixed time is depicted in Figure 3. This procedure mimics the experimental protocol used in [20] to study the size distribution of converting activity.

In case of a conversion factor $\tau(x) \equiv \tau_0$ independent of the aggregate size, the guess is simple: the more numerous are the polymers (that is the smaller is the common length y_0), the more efficient is the infection at the early stage (in the pre-exponential phase). When increasing y_0 (the total mass of PrPsc being fixed), it takes some time to fragment large aggregates into smaller ones, and the dynamics are delayed before the eventual alignment along the principal eigenfunction (in the exponential phase). This can be viewed in Figure 3 (left).

However in case of a sigmoidal conversion factor, the qualitative behavior is dramatically different. When increasing the initial aggregates' size, the infection goes through a maximal efficiency for an intermediate length (Figure 3). This is due to the inhomogeneous converting activity: it balances the disadvantage of having less but larger polymers (the total mass of PrPsc being fixed). In case of a bell shaped conversion factor, one can also observe such a qualitative behavior, to a less extent (data not shown). These data strongly resemble to those obtained experimentally in [20], and confirm that a constant extension rate seems unlikely to occur.

4.2 PrPsc size-distribution

Direct numerical simulations show that the PrPsc size-distribution is mainly affected by a non-constant conversion rate $\tau(x)$ (at the equilibrium as in the exponential growth, see Figure 2), a fact that cannot be observed on the accumulation profiles. Therefore, we analyze how it is possible to extract information from the size distribution.

A differential formulation. Recall from Section 2 that the infected steady state (V_∞, u_∞) is realized as the principal eigenfunction corresponding to the unique root of $\Lambda(\cdot)$. In this paragraph we present an alternative (simpler) formulation of the stationary problem (13), based on a second order differential equation. Note that we strongly use the peculiar choice for the fragmentation kernel $\kappa(x, y)$ (7).

Differentiating the equation for the microscopic distribution (13) we obtain,

$$V_\infty \frac{d^2}{dx^2}(\tau(x)u_\infty(x)) + \frac{d}{dx}((\mu(x)+\beta(x))\,u_\infty(x)) = \frac{d}{dx}\left(2\int_x^\infty \beta(y)\frac{1}{y}u_\infty(y)\,dy\right),$$
$$V_\infty \frac{d^2}{dx^2}(\tau(x)u_\infty(x)) + \frac{d}{dx}((\mu(x)+\beta(x))\,u_\infty(x)) + 2\frac{\beta(x)}{x}u_\infty(x) = 0\,. \tag{26}$$

This differential equation is complemented by the boundary conditions,

$$u_\infty(x_0) = 0\,, \quad V_\infty \frac{d}{dx}\Big|_{x=x_0}(\tau(x)u_\infty(x)) = 2\int_{x_0}^\infty \frac{\beta(y)}{y}u_\infty(y)\,dy\,. \tag{27}$$

The first order initial condition can be replaced by sufficient decay conditions at infinity (for instance, one moment is required for the distribution $u_\infty(x)$, at least). The problem (26–27) is linear with respect to u_∞: the missing factor ϱ_∞ (namely the total number of polymers) is determined using the first equation of (13), as in Section 2.

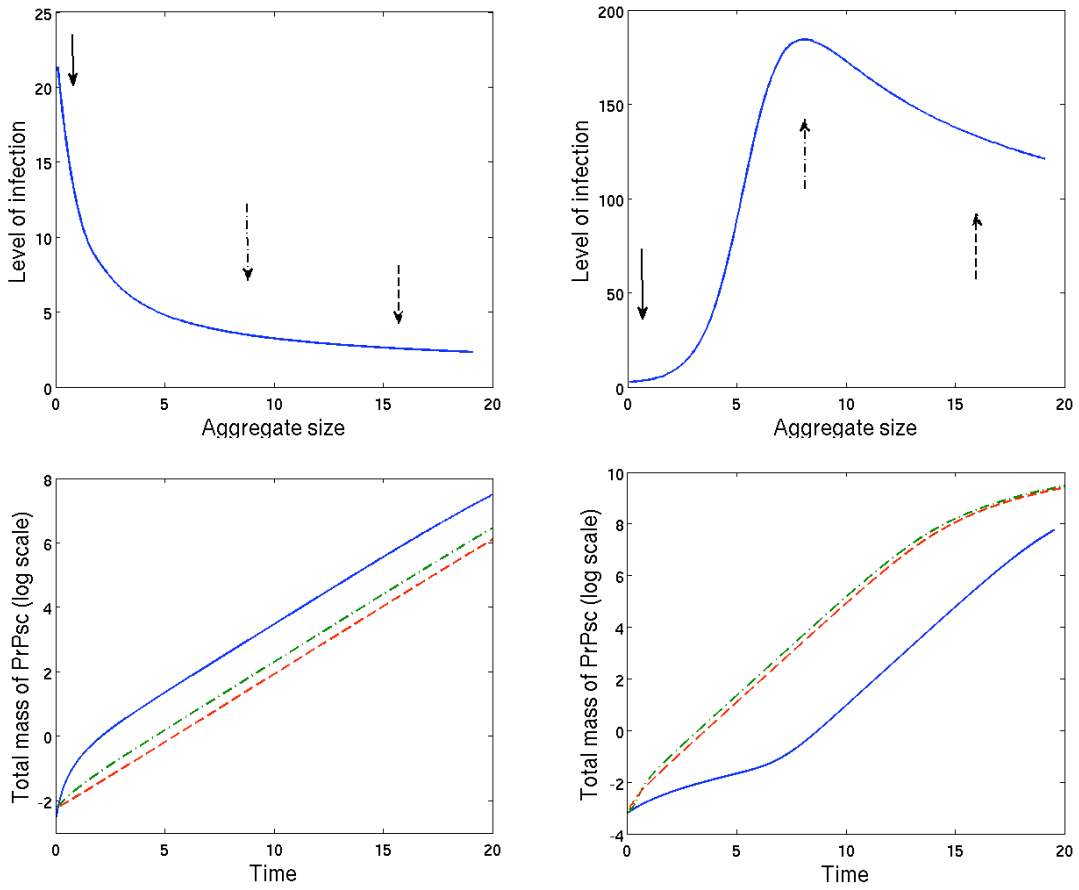

Figure 3: In silico experiments to capture the features of the conversion factor. (top) We report the quantity of PrPsc for a reference time t^* in the exponential phase ("level of infection"), as a function of the initial aggregate size (in the numerical experiments, all polymers have the same length initially, for a normalized total mass of PrPsc). (left) In case of a constant conversion rate $\tau(x) \equiv 1.10^{-2}$, this illustrates the delay in the infection dynamics that occurs when increasing initial size. (right) In case of a sigmoidal conversion rate $\tau(x) = 1.10^{-3} + 5.10^{-2} e^{x-10}/(1+e^{x-10})$, the dynamics reach a maximal efficiency for intermediate sizes. (bottom) Time evolution of the total mass of PrPsc (log scale) for three different sizes of initial aggregates corresponding to the two preceding scenarios: $y_0 = 1$ (full line), $y_0 = 8$ (dashed line), $y_0 = 16$ (dash-dotted line). One clearly distinguishes the different phases: pre-exponential phase (dynamics of the linearized system (12)), exponential phase (microscopic distribution aligned along the principal eigenfunction)... The fragmentation rate is $\beta(x) \equiv 3.10^{-2} x$ and the degradation rate is $\mu(x) \equiv 0$ to avoid the artifact of large aggregates being rapidly degraded (in fact this is a minor effect: one can choose $\mu(x) \equiv 5.10^{-2}$, data not shown).

The advantages of the differential reformulation (26) are two-folds. Firstly it provides a more efficient numerical scheme to compute the stationary distribution u_∞ because it avoids convolutions. Secondly, it dramatically simplifies the inverse problem (computing the conversion factor $\tau(x)$ from the knowledge of the distribution u_∞). According to (13), one should evaluate the eigenvalue function $\Lambda(\cdot)$, and find the root V_∞ (for example using a robust dichotomy method, based on the decreasing property of $\Lambda(\cdot)$). Alternatively, one can perform a shooting method to solve (26), matching the required decay at infinity for instance. On the other hand the inverse problem which consists in finding $\tau(x)$ from the stationary distribution $u_\infty(x)$ (given the other coefficients V_∞, $\mu(x)$ and $\beta(x)$) can be solved explicitly, integrating twice (26). However, one shall take care of the decay conditions at infinity when integrating by parts.

In some particular situations, simple mathematical considerations based on the reformulation (26) allow us to deduce some qualitative information relating the microscopic distribution and the conversion factor $\tau(x)$. In this paragraph we assume $\mu(x) \equiv \mu_0$ and $\beta(x) = \beta_0 x$ for the sake of clarity.

The second order formulation (26) is reminiscent of the standard one-dimensional Fokker-Planck equation. In fact, if we drop the last term of order 0, it becomes

$$V_\infty \frac{d}{dx}\left(\tau(x)\frac{d}{dx}v(x)\right) + \frac{d}{dx}\left(v(x)\frac{d}{dx}\psi(x)\right) = 0\,,$$

where v denotes the unknown (instead of u_∞ to avoid confusions). This accounts for an inhomogeneous diffusion with an effective confinement potential given by $\psi(x) = V_\infty\tau(x) + \mu_0 x + \frac{1}{2}\beta_0 x^2$ and its solution is $v(x) = v_0 e^{\phi(x)}$ with $\phi'(x) = -\psi'(x)/(V_\infty\tau(x))$. In the case of a sharp bell function $\tau(x)$ one can clearly see the splitting effect of the "potential" $\tau(x)$ in comparison to the "constant coefficients case" which reduces to a gaussian distribution: the natural expectation is thus a bimodal distribution.

We can go further and find necessary conditions on τ leading to a bimodal microscopic distribution u_∞, *i.e.* the distribution has two peaks, as in Figure 1 (top)). We evaluate the derivatives in the microscopic equilibrium equation (26),

$$V_\infty\left(\tau(x)\frac{d^2}{dx^2}u_\infty(x) + 2\frac{d}{dx}\tau(x)\frac{d}{dx}u_\infty(x) + \frac{d^2}{dx^2}\tau(x)u_\infty(x)\right) + \mu_0\frac{d}{dx}u_\infty(x) + \beta_0 x\frac{d}{dx}u_\infty(x) = -3\beta_0 u_\infty(x)\,.$$

A bimodal size distribution u_∞ possesses a critical point x^* where it is convex. Evaluating above expression at x^* leads to $V_\infty\tau_{xx}(x^*)u_\infty(x^*) < -3\beta_0 u_\infty(x^*)$. A necessary condition on $\tau(x)$ for the existence of such a critical point is therefore

$$\inf_{x>0} V_\infty\frac{d^2}{dx^2}\tau(x) < -3\beta_0\,.$$

It is rather intricate because V_∞ itself depends on $\tau(x)$. But it gives a first insight of the desirable conditions, meaning that $\tau(x)$ should have a peak which is concave enough.

4.3 Size distribution and strain adaptation

The analysis performed above is mainly interested in long-time dynamics resulting in an equilibrium. However, during the time course of incubation period and clinical stage of prion diseases, PrPsc accumulation in brain seems to follow an exponential dynamic until the death. Consequently, we focus here on the dynamic of PrPsc size distribution in the early stages of the polymerization process named 'exponential phase'. As mentioned in Section 2, for a given level of $\mathbf{V}$, we expect that the PrPsc size distribution tends to align along

the eigenfunction $\mathcal{U}(\mathbf{V};x)$ (the "exponential phase"). But when the initial distribution of polymers is not proportional to this eigenfunction, it induces some delay for this distribution to reach the appropriate shape, which slows down the process of prion accumulation (the "pre-exponential phase").

This property is clearly observed on numerical simulations and mimics the strain adaptation mechanism, where primary inoculation is associated with more prolonged incubation period than subsequent passages in the same type of hosts [43]. This phenomena is illustrated in Figure 4. Indeed, the eigenfunction depends upon the various parameters of the model. In particular, it depends upon the relation between the host and the prion strain as the conversion rate τ and the fragmentation rate β. When a strain is inoculated to a new host, these parameters are changed and this leads to a new eigenfunction in the equation. We can observe on the numerical simulation that the closer is the initial host distribution to the new one, the faster the accumulation is.

5 Conclusion and perspectives

Our motivation for this work is to better understand the mechanism of prion replication by nucleated polymerization. Experiments argue are in favor of size-dependent properties of PrPsc aggregates (from small oligomer to large polymers), such as the identification of distinct morphologies [20, 22] or the analysis infectivity. We therefore generalized existing mathematical model of prion replication to take into account aggregate size-dependent parameters, thus extending previous studies [9, 16, 17]. We made the choice of varying the extension rate τ for several reasons. First, in vitro conversion abilities, which is the most direct measure of τ, is heterogeneous with regards to prion aggregates size [27, 20]. Furthermore, the hypothesis of a constant extension rate rests on the fibrillar aspect of PrPsc aggregates (i.e. polymerization occurs only at two ends of the polymer)[9, 16, 17]. However, PrPsc-containing fibrils are supposed to be preparation artifacts [28, 29]. The other parameters are also expected to be size-dependent, however the model is rather difficult to attack. For further modifications concerning model (2), we suggest to take into account saturation in the fragmentation rate for large fibrils, as noticed in [20].

First, we have analysed the stability of the steady states in a general framework. The difficulty arising here is that we cannot reduce the study to a set of Ordinary Differential Equations, as it is the case in [16, 18]. Under general assumptions on the coefficients, the asymptotic stability of the healthy state (i.e. no prion aggregates) is established when the PrPc is low. We also prove that this healthy state is unstable when the PrPc production rate is high enough. This is in accordance with the asymptotic stability of the non-zero steady state for 'constant coefficients' proved in [16], even though a perfect dichotomy between the two results is left open in the general case. Biologically, these results can be interpreted as the propensity of PrPsc aggregates to give rise to prion disease depends on the amount of PrPc. This effect is known for prion diseases, where PrPc is necessary for infection [44]. However, in the more general context of understanding why some amyloids are infectious and others are not, it therefore could be useful to investigate the amount of amyloidogenic precursors.

Furthermore, we have investigated numerically in what sense a non-constant conversion rate may influence the mechanism of prion replication. Whereas changing the extension rate shape leads to similar PrPsc accumulation kinetics, the resulting equilibrium size-distributions are qualitatively very different. It is worth noticing that experimental distribution of PrP may not correspond to a steady state of the system since the biological process is dramatically stopped with the animal death. Therefore the considerations about the stationary distribution might be not biologically relevant. Nevertheless we also observe different distribution generically along the temporal dynamics.

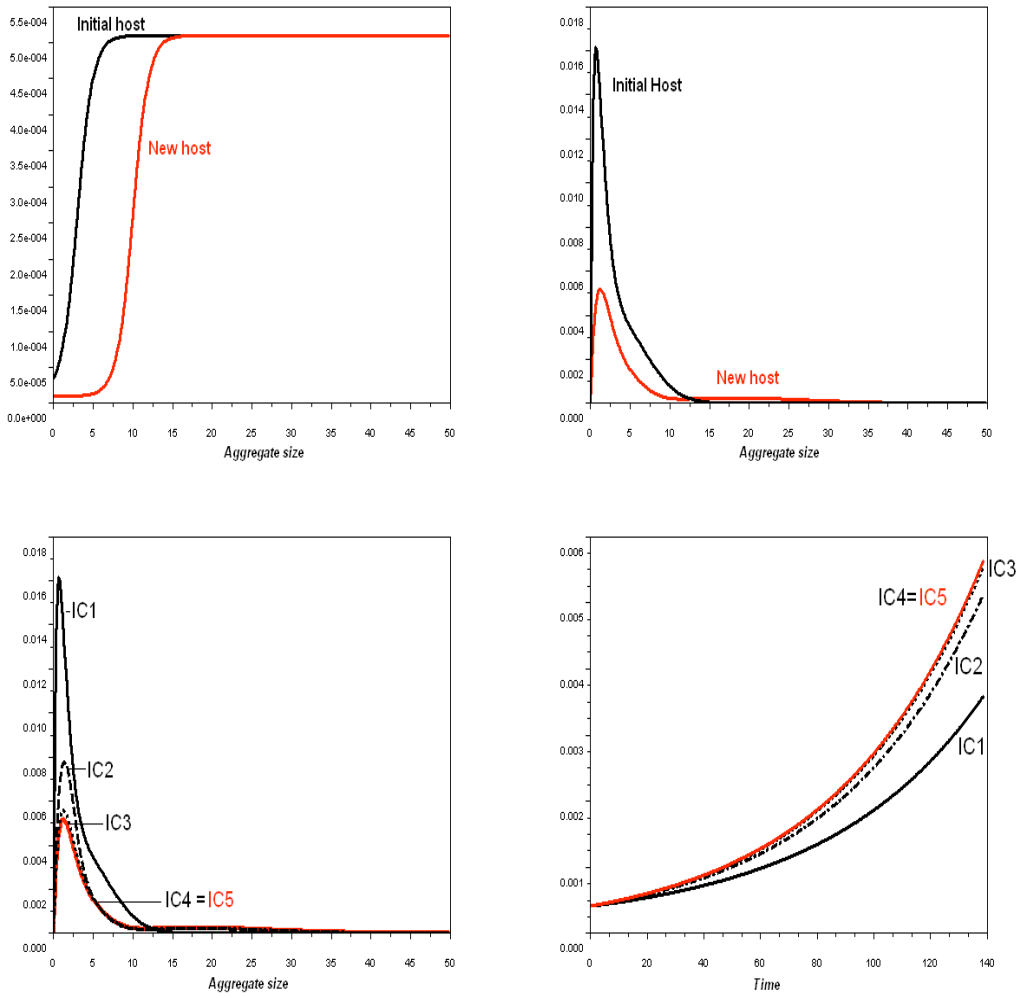

Figure 4: Prion strain adaptation. A strain is passaged from one specie, to another one. It is supposed here that changing the host leads to different conversion and fragmentation rates, the other model parameters being equal. The effect is to significantly change the size distributions. (top,left) Size distribution of the conversion rate. (top, right) Corresponding preferential size distribution, i.e., the eigenfunction $\mathcal{U}(\mathbf{V}_\infty; x)$. (bottom, left) Five initial PrPsc size-distributions have been tested in the new host. IC1 corresponds to the eigenfunction of the initial host. Each other initial condition (IC) corresponds to the final distribution obtained for the previous IC, normalized to obtain the same initial PrPsc total amount. In each case, V is initially equal to λ/γ, corresponding to the PrPc level without infection. (abscissa = PrPsc aggregates size; ordinate = PrPsc aggregates number). (bottom, right) Corresponding PrPsc accumulation kinetics (abscissa = time; ordinate = PrPsc total amount). Parameters used for the numerical simulation – Host 1 : $\tau = .00001 + .0005 * \exp(x(x-3)/(1+\exp(x-3))$ per day; $\beta = 0.03x$ per day – Host 2 : $\tau = .00001 + .0005 * \exp(x(x-10)/(1+\exp(x-10))$ per day ; $\beta = 0.003x$ per day – Hosts 1 and 2 : $\lambda = 2400$ per day, $\gamma = 4$ per day, $\mu = 0$ per day.

Based on this dynamics, we have expressed a possible explanation of the prion strain adaptation mechanism. Prion adaptation occurs during subsequent serial passages in the new host and leads to a reduction (until stabilization) of the incubation period. Nowadays, a large body of literature suggests that differences between prion strains lie in the diversity of structures of PrPsc aggregates [6, 7, 43, 45, 46, 47, 48, 49, 50]. However, the biophysical basis of strain adaptation is not well understood. Here, we just suppose that replicative parameters are different from one host to another one (due to different cofactors or different matches between donor PrPc and PrPsc conformation for instance). We show that progressive changes of the macroscopic PrPsc size distribution only can account for the adaptation. One limit to our approach is that prion strains are not only characterized by a precise incubation time but also by a specific cellular tropism. It would be of interest to introduce some mathematical formalism taking into account cell heterogeneity in the brain and the resulting local PrPsc distributions.

Taken together, our results emphasizes the potential importance of the size distribution of PrPsc aggregates, which could be very informative on prion replication mechanism. Therefore, we have shown that, in particular cases, qualitative shape of size-distribution permits deducing some information about the most converting PrPsc aggregates. These results remain purely theoretical. However, the achievement of experimental size distribution of PrPsc aggregates could allow us to approximate faithfully the inverse problem in order to obtain the size dependence of the conversion rate from the PrPsc repartition. It would therefore be possible to deduce replicative parameters, with no supplementary experiments (such as bioassays to assess incubation time for each aggregate size). Notably, we therefore would be able to determine the most infectious compartments. This knowledge is a critical step for therapeutic perspectives (where PrPsc aggregates have to be stabilized in other compartment) as for diagnostic tools, such Protein Misfolding Amplification (PMCA) [4]. PMCA goal is to quickly synthesize in vitro large amounts of PrPsc starting with minute amounts of prions. The yield of this technique is very sensitive to experimental procedures. Then size distribution of infectivity could help to optimize PMCA protocols, notably by adapting incubation and sonication steps to fall into the most converting size compartment of PrPsc aggregates.

Acknowledgements. *This work has been achieved during a visit of DO within the DEASE project (Marie Curie Early Stage Training multi Site (mEST) of the EU, MEST-CT-2005-021122).*
We would like to sincerely thank J. Silveira, A. Hughson and B. Caughey for their experimental data about PrP distribution. We are also grateful to M. Doumic for fruitful discussions. This work would not have been achieved without the help of H. Zaag.

References

[1] A. Aguzzi, *Prion diseases of humans and farm animals: epidemiology, genetics, and pathogenesis*, J. Neurochem. **97**, 1726–1739 (2006).

[2] S.B. Prusiner, M.R. Scott, S.J. DeArmond and F.E. Cohen, *Prion protein biology*, Cell **93**, 337–348 (1998).

[3] G. Legname, I.V. Baskakov, H.-O.B. Nguyen, D. Riesner, F.E. Cohen, S.J. DeArmond and S.B. Prusiner, *Synthetic mammalian prions*, Science **305**, 673–676 (2004).

[4] J. Castilla, P. Saa, C. Hetz and C. Soto, *In vitro generation of infectious scrapie prions*, Cell **121**, 195–206 (2005).

[5] H. Fraser and A.G. Dickinson, *Agent-strain differences in the distribution and intensity of grey matter vacuolation*, J. Comp. Path. **83**, 29–40 (1973).

[6] N.J. Cobb and W.K. Surewicz, *Prion strains under the magnyfying glass*, Nat. Struct. Mol. Biol. **14**, 882–884 (2007).

[7] R. Morales, K. Abid and C. Soto, *The prion strain phenomenon: molecular basis and unprecedented features*, Biochim. Biophys. Acta **1772**, 681–691 (2007).

[8] M. Eigen, *Prionics or the kinetic basis of prion diseases*, Biophys. Chem. **63**, A1–A18 (1996).

[9] J. Masel, V.A.A. Jansen and M.A. Nowak, *Quantifying the kinetic parameters of prion replication*, Biophys. Chem. **77**, 139–152 (1999).

[10] D.L. Mobley, D.L. Cox, R.R.P. Singh, R.V. Kulkarni and A. Slepoy, *Simulations of oligomeric intermediates in prion diseases*, Biophys. J. **85**, 2213–2223 (2003).

[11] R.J.H. Payne and D.C. Krakauer, *The paradoxical dynamics of prion disease latency*, J. Theoret. Biol. **191**, 345–352 (1998).

[12] R. Rubenstein, P.C. Gray, T.J. Cleland, M.S. Piltch, W.S. Hlavacek, R.M. Roberts, J. Ambrosiano and J.-I. Kim, *Dynamics of the nucleated polymerization model of prion replication*, Biophys. Chem. **125**, 360–367 (2007).

[13] F.E. Cohen, K.M. Pan, Z. Huang, M. Baldwin, R.J. Fletterick and S.B. Prusiner, *Structural clues to prion replication*, Science **264**, 530–531 (1994).

[14] J.T. Jarrett and P.T. Lansburry, *Seeding one dimensional crystallization of amyloid: a pathogenic mechanism in Alzheimer's disease and scrapie?*, Cell **73**, 1055–1058 (1993).

[15] R.V. Kulkarni, A. Slepoy, R.R.P Singh, D.L. Cox and F. Pazmandi, *Theoretical modeling of prion disease incubation*, Biophys. J. **85**, 707–718 (2003).

[16] M.L. Greer, L. Pujo-Menjouet and G.F. Webb, *A mathematical analysis of the dynamics of prion proliferation*, J. Theoret. Biol. **242**, 598–606 (2006).

[17] H. Engler, J. Pruss, and G.F. Webb, Analysis of a model for the dynamics of prions II, J. Math. Anal. Appl. **324**, 98–117 (2006).

[18] M.L. Greer, P. Van den Driessche, L. Wang and G.F. Webb, *Effects of general incidence and polymer joining on nucleated polymerization in a model of prion proliferation*, SIAM J. Appl. Math. **68** (1), 154–170 (2007).

[19] J. Pruss, L. Pujo-Menjouet, G.F. Webb, and R. Zacher, *Analysis of a model for the dynamics of prions*, Discrete Cont. Dyn. Sys. - Ser. B **6**(1), 215–225 (2006).

[20] J.R. Silveira, G.J. Raymond, A.G. Hughson, E.R. Richard, V.L. Sim, S.F. Hayes and B. Caughey, *The most infectious prion protein particles*, Nature **437**, 257–261 (2005).

[21] M. Jeffrey, C.M. Goodsir, M.E. Bruce, P.A. McBride and J.R. Fraser, *In vivo toxicity of prion protein in murine scrapie: ultrastructural and immunogold studies*, Neuropath. and Appl. Neurobio. **23**, 93–101 (1997).

[22] D. El Moustaine, V. Perrier, L. Smeller, R. Lange and J. Torrent, *Full-length prion protein aggregates to amyloid fibrils and spherical particles by distinct pathways*, FEBS Journal. **275**, 2021–2031 (2008).

[23] A.D. Snow, T.N. Wight, D. Nochlin, Y. Koike, K. Kimata, S.J. DeArmond and S.B. Prusiner, *Immunolocalization of heparan sulfate proteoglycans to the prion protein amyloid plaques of Germstmann-Straussler Syndrome, Creutzfedt-Jakob Disease and Scrapie*, Laboratory Investigation **63**, 601–611 (1990).

[24] P. Weber, A. Giese, N. Piening, G. Mitteregger, A. Thomzig, M. Beekes and H.A. Kretzschmar, *Cell-free formation of misfolded prion protein with authentic prion infectivity*, Proc. Natl. Acad. Sci. USA , 257–261 (2006).

[25] P. Weber, A. Giese, N. Piening, G. Mitteregger, A. Thomzig, M. Beekes and H.A. Kretzschmar, *Generation of genuine prion infectivity by serial PMCA*, Vet. Microbiol. **123**, 346–357 (2007).

[26] P. Weber, L. Reznicek, G. Mitteregger, H. Kretzschmar and A. Giese, *Differential effects of prion particle size on infectivity in vivo and in vitro*, Biochem. and Biophy. Res. Comm. **369**, 924–928 (2008).

[27] B. Caughey, D.A. Kocisko, G.J. Raymond and P.T. Lansbury, *Aggregates of scrapie-associated prion protein induce the cell-free conversion of protease-sensitive prion protein to the protease-resistant state*, Chemistry and Biology. **2**, 808–817 (1995).

[28] M.P. McKinley, R.K. Meyer, L. Kenaga, F. Rahbar, R. Cotter, A. Serban and S.B. Prusiner, *Scrapie prion rod formation in vitro requires both detergent extraction and limited proteolysis*, J. Virol. **65**, 1340–1351 (1990).

[29] J. Tatzelt, D.F. Groth, M. Torchia, S.B. Prusiner, S.J DeArmond, *Kinetics of prion protein accumulation in the CNS of mice with experimental scrapie*, J. Neuropath. Exp. Neurol. **58**, 1242–1249 (1999).

[30] M. Escobedo, P. Laurençot and S. Mischler, *Fast reaction limit of the discrete diffusive coagulation-fragmentation equation*, Comm. Partial Differential Equations **28**, 1113–1133 (2003).

[31] P. Laurençot and S. Mischler, *From the discrete to the continuous coagulation-fragmentation equations*, Proc. Roy. Soc. Edinburgh Sect. A **132**, 1219–1248 (2002).

[32] M. Escobedo, S. Mischler and M. Rodriguez Ricard, *On self-similarity and stationary problem for fragmentation and coagulation models*, Ann. Inst. H. Poincaré Anal. Non Linéaire **22**, 99–125 (2005).

[33] B. Perthame, Transport equations in biology, Frontiers in mathematics, Birkhäuser (2007).

[34] P. Michel, *Existence of a solution to the cell division eigenproblem*, Math. Models Methods Appl. Sci. **16**, 1125–1153 (2006).

[35] P. Michel, S. Mischler and B. Perthame, *General relative entropy inequality: an illustration on growth models*, J. Math. Pures Appl. **84**, 1235–1260 (2005) .

[36] P. Laurençot and C. Walker, *Well-posedness for a model of prion proliferation dynamics*, J. Evol. Equ. **7**, 241–264 (2007).

[37] G. Simonett and C. Walker, *On the solvability of a mathematical model for prion proliferation*, J. Math. Anal. Appl. Vol. **324** (1), 580–603 (2006).

[38] C. Walker, Prion proliferation with unbounded polymerization rates, Proceedings of the Sixth Mississippi State - UBA Conference on Differential Equations and Computational Simulations, Starkville, Mississippi, USA, Electr. J. Diff. Eqs., Conference 15, 2007.

[39] J. Pruss, R. Schnaubelt, and R. Zacher, Mathematische Modelle in der Biologie, Deterministische Homogene Systeme, Mathematik Kompakt, Birkhauser, Basel, Boston, Berlin, 2008.

[40] J.A.J. Metz and O. Diekmann, The dynamics of physiologically structured populations, Lecture notes in biomathematics, Springer-Verlag (1986).

[41] B. Perthame and L. Ryzhik, *Exponential decay for the fragmentation or cell-division equation*, J. Differential Equations **210**, 155–177 (2005).

[42] J.A. Carrillo, S. Cuadrado and B. Perthame, *Adaptive dynamics via Hamilton-Jacobi approach and entropy methods for a juvenile-adult model*, Math. Biosci. **205**, 137–161 (2007).

[43] J. Collinge and A.R. Clarke, *A general model of prion strains and their pathogenicity*, Science **318**, 930–936 (2007).

[44] H. Bueler, A. Aguzzi, A. Sailer, R.A. Greiner, P. Autenried, M. Aguet and C. Weissmann, *Mice devoid of PrP are resistant to scrapie*, Cell **73**, 1339–1347 (1993).

[45] J. Safar, H. Wille, V. Itri, D. Growth, H. Serban, M. Torchia, F.E. Cohen and S.B. Prusiner, *Eight prion strains have PrPsc molecules with different conformations*, Nat. Med. **4**, 1157–1165 (1998).

[46] G. Legname, H-O.B. Nguyen, D. Peretz, F.E. Cohen, S.J. DeArmond and S.B. Prusiner, *Continuum of prion protein structures enciphers a multitude of prion isolate-specified phenotypes*, Proc. Natl. Acad. Sci. USA **103**, 19105–10 (2006).

[47] C.J. Sigurdson, K.P.R Nilsson, S. Hornemann, G. Manco, M. Polymenidou, P. Schwarz, M. Leclerc, P. Hammarstrom, K. Wuthrich and A. Aguzzi, *Prion strain discrimination using luminescent conjugated polymers*, Nat. Methods **4**, 1023–1030 (2007).

[48] N. Makarava, C.I. Lee, V.G. Ostapchenko and I.V. Baskakov, *Highly promiscuous nature of prion polymerization*, J. Biol. Chem. **282**, 36704-13 (2007).

[49] A.M. Thackray, L. Hopkins, M.A. Klein and R. Budjoso, *Mouse-adapted ovine scrapie prion strains are characterized by diferent coformers of PrPsc*, J. Virol. **81**, 12119–27 (2007).

[50] A. Aguzzi, *Unravelling prion strains with cell biology and organic chemistry*, Proc. Natl. Acad. Sci. USA **105**, 11–12 (2008).